COMPDYN 2011
III ECCOMAS Thematic Conference on
Computational Methods in Structural Dynamics and Earthquake Engineering
M. Papadrakakis, M. Fragiadakis, V. Plevris (eds.)
Corfu, Greece, 25–28 May 2011

ANALYTICAL MODEL VERSUS NUMERICAL MODEL IN STRESS-STRAIN ANALYSIS OF BURIED STEEL PIPELINES SUBJECTED TO FAULT DISPLACEMENTS

Oleg V. Trifonov[1], **Vladimir P. Cherniy**[2]

[1,2] All-Russian research institute for natural gases and gas technologies (GAZPROM VNIIGAZ)
Razvilka poselok, Leninsky district, 142717, Moscow region, Russian Federation
{O_Trifonov, V_Cherniy }@vniigaz.gazprom.ru

Keywords: Buried steel pipeline, Active fault, Nonlinear stress analysis, Plastic strains, Pipe-soil interaction

Abstract. *In the present paper the results of the analytical model for a nonlinear stress-strain analysis of buried steel pipelines at active fault crossings are analyzed and discussed versus the numerical finite element results. The analytical model is based on the partition of the pipeline into four segments. The two segments in high curvature zones on both sides of the fault are modeled as beams in bending and tension with direct account for the axial force in the equations of motion. The two other segments are treated as beams-on-elastic foundation. The interaction of the pipeline with the surrounding soil is taken into account in axial and transverse directions using bilinear soil diagrams. The nonlinearity of the pipe steel is introduced on a cross-section level assuming a bilinear stress-strain relationship. The analysis is performed iteratively as a series of elastic solutions using a secant modulus of the pipe steel. The analysis of applicability of the proposed model to various cases of pipeline-fault intersection conditions is performed through the comparison of the results obtained with the analytical model to the results of the numerical simulation of the finite element model in ANSYS. The developed finite element model uses current technology ANSYS pipe elements with account for axial, bending, shear and torsional deformations, material nonlinearity, large displacements and strain nonlinearities. The pipe-soil interaction is modeled by the nonlinear soil spring elements. The analysis of the results allows drawing the conclusion on the applicability of the proposed analytical methodology to a wide range of conditions met in practice, at least for the preliminary assessment. The limitations of the analytical methodology and possible further refinements are also discussed.*

1 INTRODUCTION

The advancement of the gas-transport systems to the regions of high seismic activity reinforces the actuality of the research in the field of seismic analysis and design of main gas pipelines. The research methods in stress-strain analysis of pipelines can be generally divided into analytical and numerical. Giving credit for a progress in numerical finite and boundary element methods, we still have to admit the actuality of analytical models which are well suited for preliminary analysis and provide basis for more advanced numerical techniques.

It is well known that permanent ground deformation caused by relative displacements of adjacent parts of earth's crust along the fault is among the most dangerous earthquake effects and can result in a pipe failure [1]. The first paper considering a fault crossing problem analytically was published by Newmark and Hall [2]. A case of pipeline intersecting a strike-slip fault at an angle $\beta \le \pi/2$ is studied. The axial strain component is considered to have the major effect on the pipeline. The average axial tensile strains along the effective unanchored length are calculated using the pipeline elongation due to the axial component of the fault movement and due to the second-order effects caused by lateral component of the fault movement. Since the bending stiffness and lateral pipe-soil interaction is neglected and the axial strains are averaged over the unanchored length, the maximal strains are underestimated.

Later, Kennedy et al. [3] extended the methodology proposed in [2]. The bending strains are introduced into the model based on a cable schematization. Given this assumption, adequate results can only be obtained in the case of large fault movements in projection on the axial pipe direction producing substantial axial tensile strain component.

Further advancements to the analytical models for a pipeline crossing strike-slip fault were made by Wang and Yeh [4]. Their model is based on a division of a pipe into four segments. The two segments in high curvature zone on both sides of the fault trace act as circular arcs, while the two other segments are considered as beams-on-elastic-foundation. The most significant shortcoming of the model is that the influence of axial force on the bending stiffness is neglected. Also, according to the model, the critical combination of the axial and bending strains develops at the ends of high curvature zones on each side of the fault. On the contrary, it can be shown [5, 6] that the maximal stresses and strains develop within these zones, closer to the fault intersection point.

Recently, Karamitros et al. [5] introduced a number of substantial refinements to the above mentioned methodology. In the model, the two segments in high curvature zones are considered within the elastic beam theory taking into account the pipe-soil interaction in both axial and transverse directions. The elastoplastic behavior of the pipe steel is considered within a bilinear stress-strain relationship. The analysis is performed iteratively as a series of elastic solutions using a secant modulus of the pipe steel. The results of the developed model show good agreement with the finite element results for strike-slip fault crossings over a range of fault displacements $\Delta = 0 \div 2D$, where D is the pipe diameter, and the intersection angles $\beta = 30^0, 45^0$ and 60^0.

Some essential shortcomings of the previous methodologies are addressed in the paper by Trifonov and Cherniy [6]. In particular, no symmetry condition about the intersection point is used, allowing for different types of fault kinematics to be analyzed; the tension-bending interaction is taken into account directly in the equations of motion of the two segments in high curvature zones on both sides of the fault; the contribution of transverse displacements to the axial elongation is included in calculation of axial stresses and strains. A good agreement was established between the results of the developed analytical model and finite-element model for a strike-slip and normal slip fault crossing problems.

In the present work, the application of model of the paper [6] to a strike-slip fault crossing problem is analyzed in comparison to the finite element results. In the following section the analytical model is briefly discussed. Next, in section 3 the numerical finite element model developed for the verification of the analytical methodology is presented, and the comparison of the analytical to numerical finite element results is performed. The limitations of the analytical model are also discussed. Finally, in section 4 some additional corrections to the analytical model are introduced and discussed in connection with the finite element results.

2 ANALYTICAL MODEL OF A PIPELINE CROSSING ACTIVE FAULT

2.1 Structural model of a pipeline in the fault zone

Following the papers [5, 6], a pipeline is partitioned into four segments shown in figure 1. Point B represents the intersection of the pipeline with the fault trace; points A and C are the closest points of the pipeline axis with zero transverse displacements. Points A' and C' are at a distance from A and C that is sufficient for the attenuation of transverse displacements.

As the pipeline transverse displacements relative to surrounding soil are small on the segments AA' and CC', the pipe-soil interaction can be considered as elastic and a beam-on-elastic foundation theory can be applied. The pipeline transverse displacements $w(x)$ follow the equation

$$EI\frac{d^4w}{dx^4}+kw=0 \tag{1}$$

where x is the coordinate measured from the point A (or C), E is the elastic modulus, I is the moment of inertia of the cross-section, k is the stiffness parameter of the elastic foundation. Assuming that soil resistance in considered transverse direction is characterized by a bi-linear diagram with the displacement at yield w_u and corresponding force q_u, the stiffness of the elastic foundation is calculated as $k = q_u / w_u$.

The solution of the Eq. (1) is obtained with the use of the boundary conditions $w = 0$ for $x = 0$ and $w \to 0$ for $x \to \infty$:

$$w(x) = Ce^{-\lambda x}\sin\lambda x \tag{2}$$

where $\lambda = (k/4EI)^{1/4}$.

The segments AB and BC are analyzed as elastic beams loaded with the axial force F and distributed transverse load q. The intensity of the distributed load is equal to the limit value of pipe-soil interaction force per unit length for considered transverse pipe displacement direction relative to surrounding soil. This assumption is valid for the strike-slip fault crossing. In case of normal-slip fault with relatively small displacements an alternative partition accounting for elastic soil behavior on the segment with downward relative pipeline movement gives better results. The details on this case are given in the paper [6]. In the following, we will concentrate on the analysis of a strike-slip crossing problem.

The equilibrium equation for the beam under combined bending-tension can be obtained considering the equilibrium of the differential line element in the deformed configuration loaded with the constant axial force F and uniformly distributed transverse load q:

$$EI\frac{d^4w}{dx^4}-F\frac{d^2w}{dx^2}=q \tag{3}$$

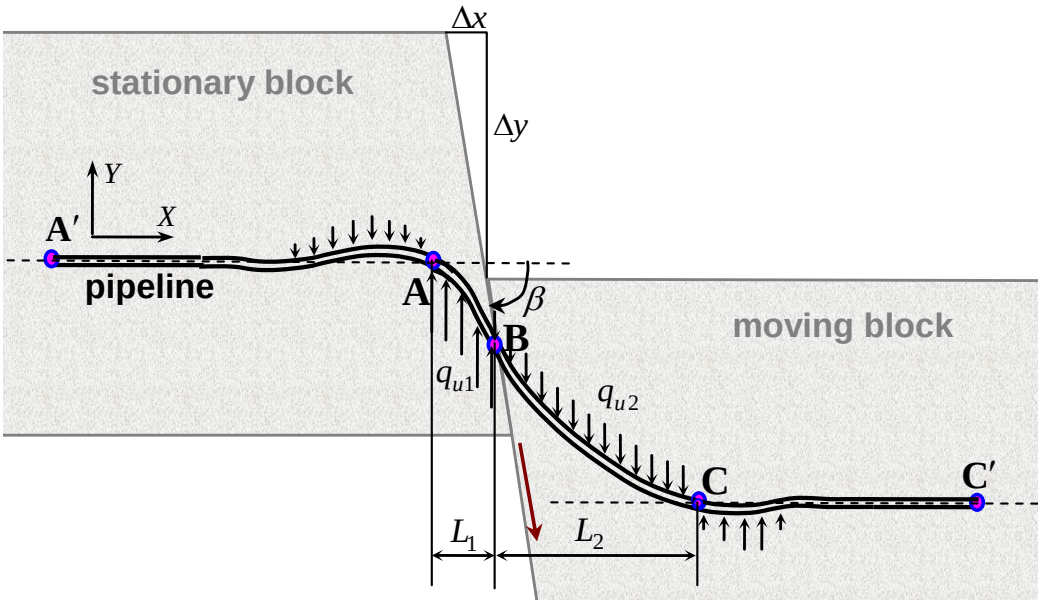

Figure 1: Pipeline model at active fault crossing.

The solution of Eq. (3) can be written in the form of initial parameters:

$$w(x) = w(0) + \phi(0)\frac{\sinh \alpha x}{\alpha} + \frac{M(0)}{EI\alpha^2}[\cosh \alpha x - 1] + \\ + \frac{V(0)}{EI\alpha^3}[\sinh \alpha x - \alpha x] + \frac{q}{F}[(\cosh \alpha x - 1)/\alpha^2 - x^2/2] \tag{4}$$

where $\alpha^2 = F/EI$. The parameters $\phi(0)$, $M(0)$, and $V(0)$ are the rotation angle, bending moment, and transverse force for the section with $x = 0$.

The unknown parameters in Eq. (2) and (4) written for the corresponding pipe segments together with the unknown length parameters L_1 and L_2, are found from the boundary conditions on the junction points A, B, and C. The resulting system of nonlinear algebraic equations can be solved numerically as shown in [6]. In the case of a strike-slip fault the pipeline-soil interaction forces acting on the segments AB and BC are identical. The use of symmetry condition in this case simplifies the resulting system of equations which reduces to a single nonlinear equation solved by the Newton-Raphson technique.

After the solution $w(x)$ is obtained, other quantities, such as rotation $\phi(x) = w'(x)$, bending moment $M(x) = EIw''(x)$ and transverse force $V(x) = EIw'''(x) - Fw'(x)$ can be evaluated (here the notation $w' = dw/dx$ is used). Also, the maximum bending moment $|M_{\max}|$ can be derived for each segment. Further details on the structural model and solution procedure can be found in [6].

2.2 Evaluation of the axial stress and strain

The axial force in Eq.(3) is assumed constant and equal to the axial force at the intersection of the pipeline with the fault trace. The latter is calculated by equating the geometrically required and the stress-induced (available) pipeline elongations.

The geometrically required elongation ΔL_{req} results from the fault movement in the axial direction and the pipeline elongation due to bending:

$$\Delta L_{req} = \Delta \cos\beta + \frac{1}{2}\int_x (w')^2 dx \tag{5}$$

where Δ is the fault displacement, β is the fault intersection angle. Integration in the second term in Eq. (5) is performed over the curved segments AB and BC.

The available elongation ΔL_{av} is evaluated by integrating the axial strains $\varepsilon_a(x)$ over the unanchored length L_{anch}, characterized by relative slippage of the pipe and the surrounding soil:

$$\Delta L_{av} = 2\int_0^{L_{anch}} \varepsilon_a(x) dx \tag{6}$$

In Eq. (6), it is assumed that the elongation on both sides of the fault trace is identical.

Denoting the axial force and axial stress developing at the fault intersection point by F_a and σ_a, the unanchored length L_{anch} can be calculated as:

$$L_{anch} = F_a / t_u = \sigma_a A_s / t_u \tag{7}$$

where A_s is the pipe cross-sectional area, and t_u is the limit pipe-soil interface friction.

The axial strain distribution over the length L_{anch} is obtained from the axial stress distribution

$$\sigma(x) = \sigma_a - t_u x / A_s \tag{8}$$

assuming a bilinear stress-strain relationship for the pipe steel:

$$\varepsilon_a(x) = \begin{cases} \sigma(x)/E, & \sigma(x) \le \sigma_Y \\ \sigma_Y / E + (\sigma(x) - \sigma_Y)/E_t, & \sigma(x) > \sigma_Y \end{cases} \tag{9}$$

In Eq. (9), E is the elastic modulus, E_t is the hardening parameter (plastic modulus), σ_Y is the yield stress.

Combining Eqs. (6), (8), and (9) and using the condition $\Delta L_{av} = \Delta L_{req}$, the axial stress at the fault intersection can be evaluated as [5, 6]:

$$\sigma_a = \begin{cases} [E t_u \Delta L_{req} / A_s]^{1/2}, & \Delta L_{req} \le \sigma_Y^2 A_s / (E t_u) \\ \sigma_Y (1 - E_t / E) + & \\ [\sigma_Y^2 ((E_t / E)^2 - E_t / E) + E_t t_u \Delta L_{req} / A_s]^{1/2}, & \Delta L_{req} > \sigma_Y^2 A_s / (E t_u) \end{cases} \tag{10}$$

2.3 Modeling of the interaction between the axial and bending strains on sectional level

If the plastic strains develop in the cross-section with the maximum bending moment, the axial and bending strains become interconnected. In particular, axial strains in the vicinity of the corresponding cross-section increase locally, ensuring the equilibrium between the stress-integrated axial force and the applied axial force. To account for this effect, the stress and strain distributions over the cross-section have to be considered [6].

Under the assumption of plane cross-sections, the strain distribution on the cross-section with the maximum bending moment is given by

$$\varepsilon = \varepsilon_a + \varepsilon_b \cos\theta \tag{11}$$

where ε_a is the axial strain, and $\varepsilon_b = M_{\max} D/(2EI)$ is the maximal bending strain, θ is the polar angle of the cross-section measured from the vertical diameter (figure 2).

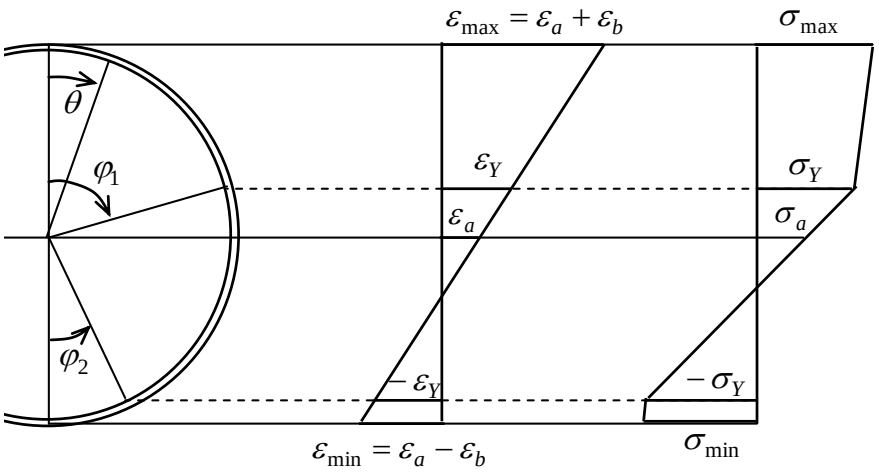

Figure 2: Stress and strain distribution over the cross-section.

In figure 2 the yield strain is denoted by ε_Y and the angles $\varphi_{1,2}$ define the portions of the cross-section that undergo yielding:

$$\varphi_{1,2} = \begin{cases} \pi, & \dfrac{\varepsilon_Y \mp \varepsilon_a}{\varepsilon_b} < -1 \\ \arccos\left(\dfrac{\varepsilon_Y \mp \varepsilon_a}{\varepsilon_b}\right), & -1 \le \dfrac{\varepsilon_Y \mp \varepsilon_a}{\varepsilon_b} \le 1 \\ 0, & 1 < \dfrac{\varepsilon_Y \mp \varepsilon_a}{\varepsilon_b} \end{cases} \tag{12}$$

Accordingly, the distribution of stresses takes the form:

$$\sigma = \begin{cases} \sigma_Y + E_t(\varepsilon - \varepsilon_Y), & 0 \le \theta < \varphi_1, \\ E\ \varepsilon, & \varphi_1 \le \theta \le \pi - \varphi_2, \\ -\sigma_Y + E_t(\varepsilon + \varepsilon_Y), & \pi - \varphi_2 < \theta \le \pi. \end{cases} \tag{13}$$

The axial force and bending moment are evaluated by the stress-integration over the cross-section with the use of Eq. (11) – (13):

$$\begin{aligned} &F(\varepsilon_a, \varepsilon_b) = 2\int_0^{\pi} \sigma R_m t d\theta = \\ &= 2R_m t[E\ \pi\varepsilon_a - (E\ - E_t)(\varphi_1 + \varphi_2)\varepsilon_a + (E\ - E_t)(\varphi_1 - \varphi_2)\varepsilon_Y - \\ &- (E\ - E_t)(\sin\varphi_1 - \sin\varphi_2)\varepsilon_b], \end{aligned} \tag{14}$$

$$M(\varepsilon_a,\varepsilon_b) = 2\int_0^{\pi} \sigma R_m t R_m \cos\theta \, d\theta =$$
$$= \tfrac{1}{2} R_m^2 t[2E\ \pi\varepsilon_b - 4(E\ - E_t)(\sin\varphi_1 - \sin\varphi_2)\varepsilon_a + \quad (15)$$
$$+ 4(E\ - E_t)(\sin\varphi_1 + \sin\varphi_2)\varepsilon_Y - 2(E\ - E_t)(\varphi_1 + \varphi_2)\varepsilon_b -$$
$$- (E\ - E_t)(\sin 2\varphi_1 + \sin 2\varphi_2)\varepsilon_b].$$

Here, the notation $R_m = (D-t)/2$ is used.

For the evaluation of the axial strain in the cross-section with the maximum bending moment the equilibrium condition between the applied axial force and the one obtained by the integration over the cross-section is used:

$$F(\varepsilon_a,\varepsilon_b) - F_a = 0 \quad (16)$$

The Eq. (16) can be treated as a nonlinear function of ε_a and solved iteratively.

To satisfy the moment equilibrium condition

$$M(\varepsilon_a,\varepsilon_b) - M_{\max} = 0 \quad (17)$$

an iterative solution is performed using the secant Young's modulus derived from the Eq. (17):

$$E_{\sec} = \frac{M(\varepsilon_a,\varepsilon_b)D}{2I\varepsilon_b} \quad (18)$$

The specified procedure is applied separately to the segments AB and BC, yielding $\varepsilon_{a1}, \varepsilon_{a2}$ and $E_{\sec 1}$, $E_{\sec 2}$, which are applied on the next iteration.

2.4 The solution algorithm

The described model can be implemented in a computer program according to the algorithm given below. For a general fault kinematics the algorithm consists of the following steps (superscript *k* stands for the iteration number):

1. Given the fault kinematics and the intersection angle, calculate the components of fault displacements in projection on the pipe coordinate system Δx and Δy.
2. Using the transverse displacements from the previous iteration $w_1^{(k-1)}(x)$ and $w_2^{(k-1)}(x)$, calculate the elongation due to the pipe transverse displacements, the required elongation $\Delta L_{req}^{(k)}$ and axial force $F_a^{(k)}$ (section 2.2).
3. Performing the solution of the structural problem (section 2.1) using the appropriate secant moduli $E_{\sec 1}^{(k)}$ and $E_{\sec 2}^{(k)}$, evaluate the lengths of the segments AB and BC $L_1^{(k)}$ and $L_2^{(k)}$. Evaluate the transverse displacements $w_1^{(k)}(x)$ and $w_2^{(k)}(x)$.
4. Find the maximum absolute values of the bending moments on segments AB and BC $M_{1\max}$ and $M_{2\max}$. Evaluate the corresponding maximum bending strains ε_{b1} and ε_{b2}.
5. Evaluate the maximum axial strains on segments AB and BC ε_{a1} and ε_{a2} performing an iterative solution of Eq.(16) for segments AB and BC.
6. Evaluate bending moments $M_1^{(k)}(\varepsilon_{a1},\varepsilon_{b1})$ and $M_2^{(k)}(\varepsilon_{a2},\varepsilon_{b2})$ on segments AB and BC.

7. Check the moment convergence. If the convergence criterion is satisfied, proceed to the next load step or terminate the solution (step 8). Otherwise, calculate secant moduli $E_{\text{sec}1}^{(k+1)}$ and $E_{\text{sec}2}^{(k+1)}$ for segments AB and BC and go to the next iteration (step 2).
8. Output the results and stop the solution.

The initial displacement functions $w_1^{(0)}(x)$ and $w_2^{(0)}(x)$ used on the first iteration ($k=1$) for calculation of $\Delta L_{req}^{(1)}$ and $F_a^{(1)}$ are taken as zero, if the total fault displacement is applied in one step, or as the displacements calculated on the previous load step, if the total fault displacement is applied in several steps. The initial values of the secant moduli $E_{\text{sec}1}^{(1)}$ and $E_{\text{sec}2}^{(1)}$ are equal to the elastic modulus E.

The convergence of the described algorithm observed during numerical modeling is rather good for different fault intersection angles and total fault displacements. The number of iterations necessary to meet the convergence criteria ranged from 1 to 7.

3 THE RESULTS OF THE ANALYTICAL MODEL VERSUS FINITE ELEMENT MODEL

3.1 Finite element pipeline model

To analyze the applicability of the analytical model to practical cases of pipeline-fault intersection conditions, a finite element model is developed. The finite element model treats a structural problem of pipeline crossing active fault more rigorously, thus, allowing the assessment of the influence of simplifying assumptions adopted in the analytical model on the stress and strain predictions. The finite element model is implemented in ANSYS 12.1 [7]. A pipeline segment with the length 1000 m is considered. The fault intersection point is placed at the middle of the segment. The pipeline is clamped at the end on the stationary part of the fault and free at the end on the moving part of the fault.

The pipeline segment is meshed by 1000 PIPE288 elements with the concentration of elements in the near-fault zone (taken as 50 m on both sides of the fault). The PIPE288 is a three-dimensional element based on Timoshenko beam theory with axial, bending, shear and torsion deformations included. Large displacements, strains, material nonlinearity are also accounted for.

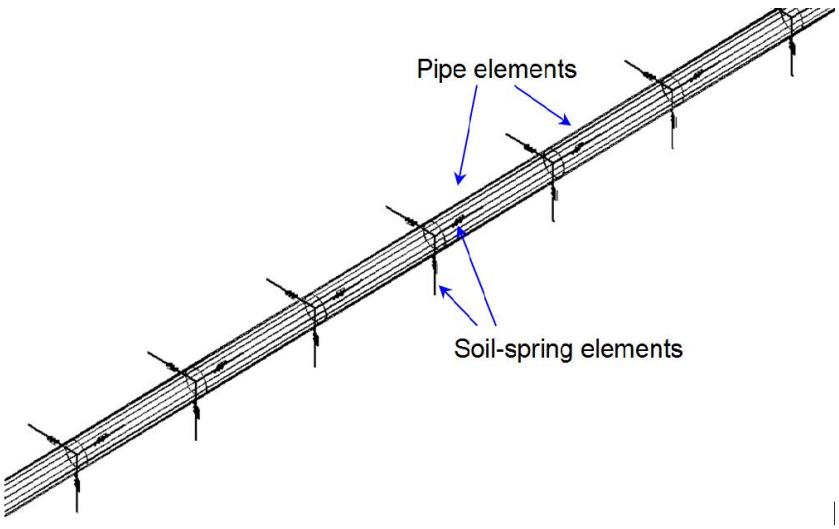

Figure 3: A fragment of the finite element model.

The pipe-soil interaction is modeled by nonlinear spring COMBIN39 elements oriented in the three orthogonal directions. The element allows for arbitrary nonlinear force-deflection curve to be used. In the analysis, an elastic-perfectly plastic diagrams with characteristics calculated according to ALA-ASCE [8] guidelines were used.

A fragment of the finite element model is depicted in figure 3.

The total fault displacement is applied in 50 steps with automatic substepping and convergence control. The fault displacement components are prescribed to the free ends of the corresponding soil-spring elements on the moving part of the fault, while the soil-spring free ends on stationary part of the fault are fixed. On each step the solution quantities are output into the data files for subsequent analysis.

3.2 Numerical results for the case of strike-slip fault crossing

The numerical examples described in this section are based on the pipeline and soil data used in the papers [5, 6]. A natural gas pipeline with the external diameter $D = 0.9144$ m, wall thickness $t = 0.0119$ m is considered. The pipeline material has the following characteristics: yield stress $\sigma_Y = 490$ MPa, elastic Young's modulus $E = 210$GPa, hardening modulus $E_t = 1.088$ GPa. The pipe-soil interaction is modeled by elastic-perfectly plastic diagrams. The corresponding parameters are calculated according to the ALA-ASCE guidelines [8] for the case of medium-density sand with friction angle 36^0, unit weight 18 kN/m^2 and pipe burial depth equal to 1.3 m.

The fault intersection angles, taken for numerical simulation in papers [5, 6], ranged from 30^0 to 60^0. A good correspondence of the analytical results to numerical results was observed. But from the practical viewpoint, the case of intersection angle close to 90^0 is an important one. Therefore, it is desirable to determine the level of accuracy of the results obtained using the proposed analytical methodology in this range of angles. The case of a strike-slip fault will be considered below as practical example.

Probably, the most representative quantity, characterizing the level of correspondence between the finite element and the analytical results, is the maximal strain in the pipe. Also, this parameter is the main characteristic used in the strain-based design procedures. Figure 4 illustrates the evolution of the maximal longitudinal strains with the fault displacement for the two values of the fault intersection angle $\beta = 30^0$ (a) and 90^0 (b). The solid line corresponds to the analytical solution while the dashed line represents the finite element solution.

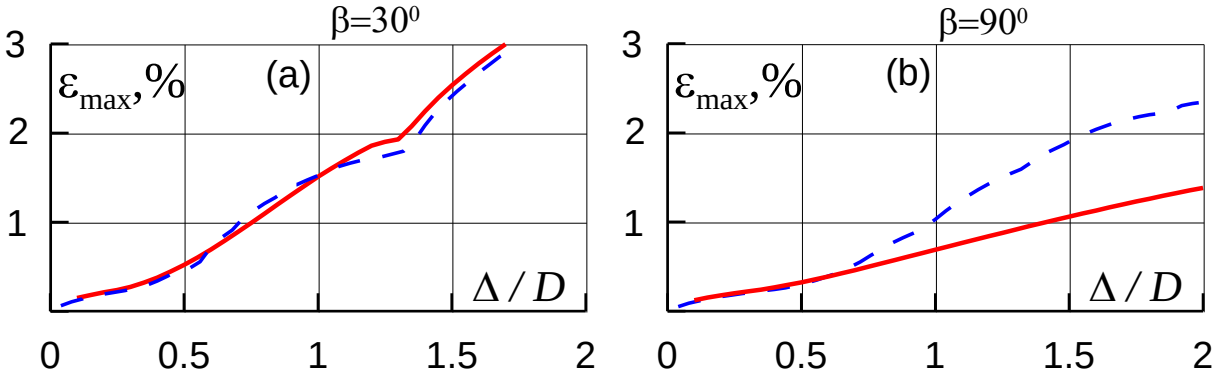

Figure 4: Comparison of the analytical (solid lines) and finite element (dashed lines) solutions for the two cases of fault intersection.

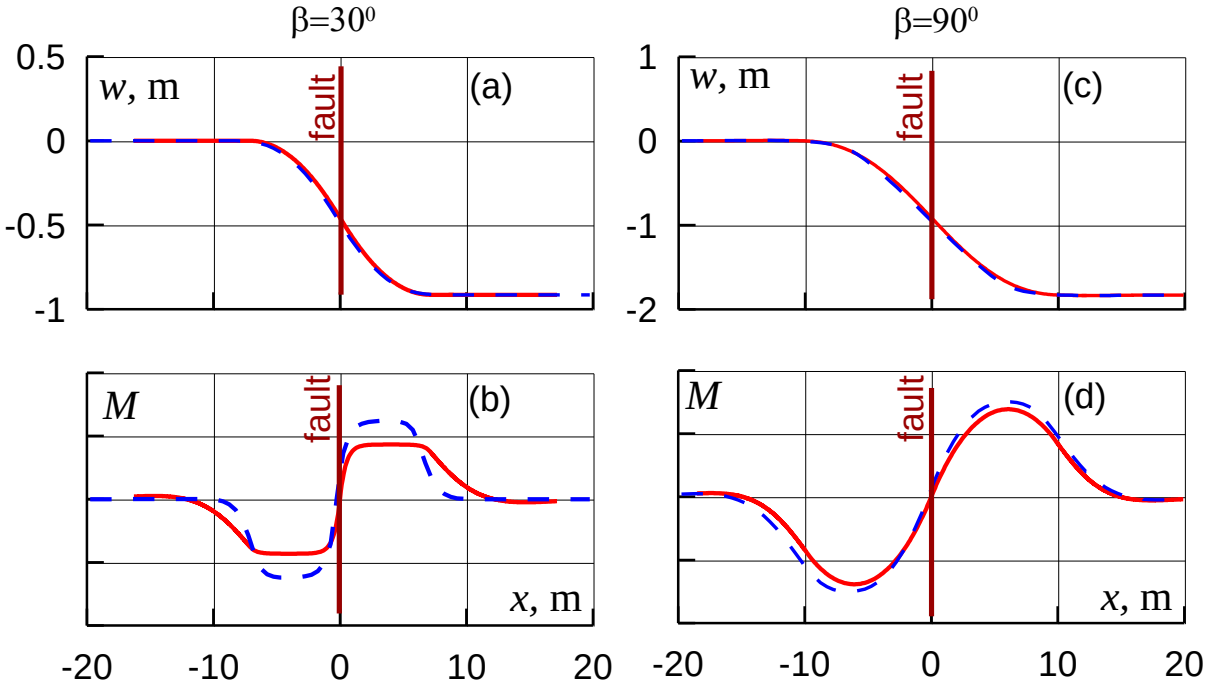

Figure 5: Distributions of the transverse displacements and bending moments in the near-fault zone.

It is seen that for the case $\beta = 30^0$ the results are rather close in the whole range of values of the fault displacements, while for the case $\beta = 90^0$ the results substantially differ starting from $\Delta / D = 0.7$. The maximal difference near 40% is observed for $\Delta / D = 2$.

To understand the cause of this discrepancy, other solution quantities were analyzed. The distributions of the transverse displacements and bending moments in the near-fault zone are depicted in figure 5. The correspondence of the finite element (dashed lines) and the analytical results is rather good in both cases.

The distributions of the longitudinal strains are shown in figure 6. Total strain is a more sensitive parameter revealing substantial differences between the rigorous numerical model and approximate analytical model for the case of $\beta = 90^0$ (figure 6, b). Surprisingly, the closeness of the results for $\beta = 30^0$ (figure 6, a) is good, especially taking into account the approximate character of the analytical model and a rather complex shape of the strain distribution. The sharp drop in strains on analytical results reflects the transition to the segments AA' and CC' considered as beams-on-elastic foundation with the initial Young's modulus.

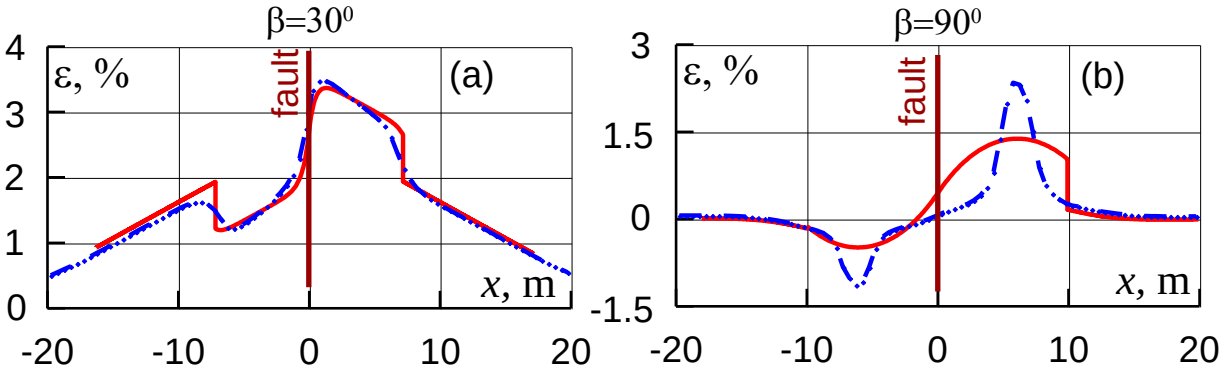

Figure 6: Distribution of the longitudinal strains in the near-fault zone.

In the case $\beta = 90^0$, numerical solution shows a concentration of deformations in relatively narrow zones on both sides of the fault. These zones do not side the fault intersection point but are rather at distance of several meters. As shown in figure 7 representing the finite element solution for plastic strains, the concentration of strains corresponds to the zones of plasticity. These zones are compact and pronounced for $\beta = 90^0$ as in this case the bending dominates, while for $\beta = 30^0$ a substantial axial component of strain causes a dramatic "stretching" of plastic zones.

In the analytical model the potentially plastic zones (segments AB and BC) are bounded by the fault intersection point and the nearest point with zero relative pipe-soil displacements in transverse direction. Thus, for $\beta = 90^0$ plastic deformations in analytical solution are spread over substantially larger length than in numerical solution. Consequently, the equivalent secant modulus is larger than the plastic modulus of the material and the maximal strains are smaller but more evenly distributed.

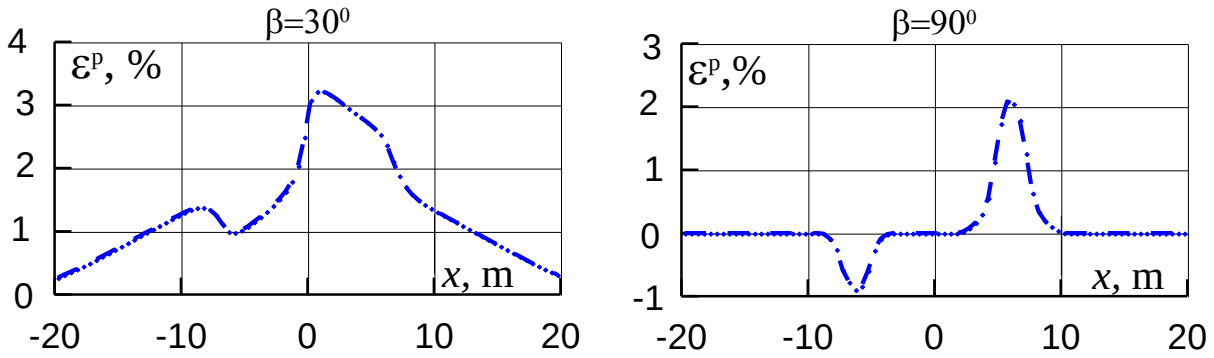

Figure 7: Distribution of the plastic strains in the near-fault zone (finite element solution).

Hence, in the situations when bending is the prevailing mechanism of deformation, the analytical model would underestimate the maximal strains. On the other hand, in situations when axial strains are significant, the analytical model would give reasonable maximal strain predictions. In the next section a correction of the analytical methodology is suggested and illustrated on numerical examples.

4 AN APPROXIMATE ACCOUNTING FOR THE STIFFNESS VARIATION WITHIN THE PROPOSED ANALYTICAL MODEL

4.1 The stiffness correction method

One of the simple ways to remedy the analytical results for the fault intersection angles close to 90^0 is based on stiffness correction within the segments AB and BC without performing any changes in the basic methodology.

For the final evaluation of strains, the initial beam is replaced by a beam with varying stiffness $EI = EI(\xi)$, where ξ is a non-dimensional coordinate within the pipeline segment. It is considered that all other loading conditions remain the same, giving an identical moment distribution along the segment. This assumption is supported by relative closeness of the moment distributions for analytical and finite element solutions shown in figure 5. Thus, it seems reasonable to state the equivalence of the bending strain energies of the initial beam with the secant stiffness and the modified beam with varying stiffness:

$$\frac{1}{2}\int_l \frac{M^2(x)}{E_{\text{sec}} I} dx = \frac{1}{2}\int_l \frac{M^2(x)}{EI(x)} dx \tag{19}$$

Next, we adopt the following approximation of the stiffness distribution:

$$EI(\xi) = aE_{\text{sec}} I - \omega(\xi)(aE_{\text{sec}} I - bE_{\text{sec}} I) \tag{20}$$

where the shape function $\omega(\xi)$ is given by

$$\omega(\xi) = \begin{cases} 0, & \xi < 0, \quad \xi > 1 \\ 16(\xi^4 - 2\xi^3 + \xi^2), & 0 \le \xi \le 1 \end{cases} \tag{21}$$

and

$$\xi = (x - x_{\max}) / l_p + 0.5 \tag{22}$$

Here, l_p is the support of the function $\omega(\xi)$, $x_{\max}$ is the position of the maximum bending moment within the segment. Parameter l_p defines the length of the concentration zone.

For $x = x_{\max}$ we have: $\xi = 0.5$, $\omega(\xi) = 1$ and $EI(\xi) = bE_{\text{sec}} I$. For $x = 0$ and $x = L$ (where L is the segment length) under the condition $l_p < L$ we have $\omega(\xi) = 0$ and $EI(\xi) = aE_{\text{sec}} I$. Thus, the amount of stiffness variation is controlled by the parameters a and b.

As the strain concentration is connected to the strain variability within the segment and becomes higher with the strain growth, it is natural to consider the dependence of the parameters *a* and *b* on:

- Maximal bending strains within the segment ε_b;
- The parameter of unevenness taken as the ratio of average bending strains to the maximum bending strains:

$$\zeta = \varepsilon_{b,av} / \varepsilon_b \tag{23}$$

where the average bending strain is calculated as

$$\varepsilon_{b,av} = \frac{1}{L}\int_0^L \varepsilon_b(x) dx \tag{24}$$

The parameter of unevenness is plotted on figure 8, a for various fault intersection angles based on the analytical solution. It is seen that this characteristic helps to differentiate the cases where the concentration is insignificant and the ones with substantial strain concentration for large fault displacements.

Picking out the bounding levels ζ_1 and ζ_2, the following secondary parameter of unevenness is introduced:

$$C_1 = \begin{cases} a_1\zeta + b_1, & \zeta < \zeta_1 \\ 1, & \zeta \ge \zeta_1 \end{cases} \tag{25}$$

where

$$a_1 = [C_1(\zeta_1) - C_1(\zeta_2)]/[\zeta_1 - \zeta_2], \; b_1 = [\zeta_1 C_1(\zeta_2) - \zeta_2 C_1(\zeta_1)]/[\zeta_1 - \zeta_2] \tag{26}$$

Here $C_1(\zeta_1)$ and $C_1(\zeta_2)$ are the values of the parameter C_1 at bounding levels taken as $C_1(\zeta_1)=1$ and $C_1(\zeta_2)=2$. The expression (25) is illustrated in figure 8, b.

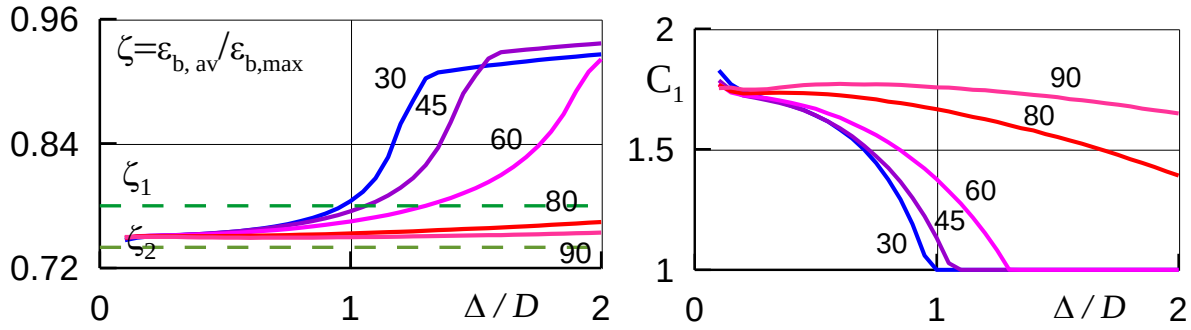

Figure 8: (a) The parameter of unevenness for various fault intersection angles. (b) Secondary parameter of unevenness.

To mitigate C_1 in the range of small strains the following parameter is used:

$$C_2 = \varepsilon_b / \varepsilon_{b,1} \tag{27}$$

where $\varepsilon_{b,1}$ – some normalizing level taken in the following equal to 0.007. The numerical values of ζ_1, ζ_2, $C_1(\zeta_1)$ and $C_1(\zeta_2)$ are based entirely on analytical solution. The numerical value of $\varepsilon_{b,1}$ defines the amount of strain concentration. Actually, this is the only parameter which is fitted using the finite element results. Finally, the following characteristic of the strain concentration is derived:

$$C_3 = \begin{cases} C_1 C_2, & C_1 C_2 > 1 \\ 1, & C_1 C_2 \le 1 \end{cases} \tag{28}$$

The evolution of this characteristic with the fault displacement is shown in figure 9.

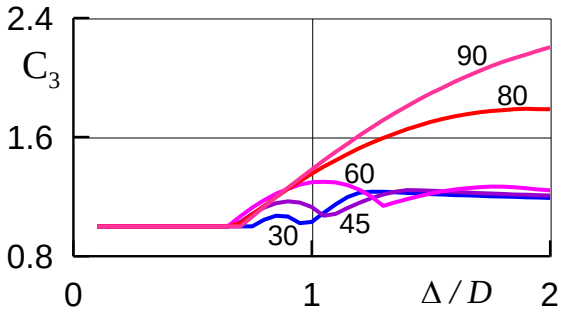

Figure 9: The characteristic of the strain concentration.

The application of the obtained strain concentration parameter within the framework of Eq. (20) is given by the relations

$$a = C_3, \quad b = 1/C_3 \tag{29}$$

Thus, in the strain concentration region the original secant stiffness is reduced in C_3 times, while outside this region it is increased in C_3 times. The proposed relations are rather approx-

imate but at least qualitatively represent the character of the actual stiffness distribution. The application of the proposed correction technique is illustrated in the following section.

4.2 Corrected solution for various fault intersection angles

Using the proposed correction procedure, the following steps within the basic solution algorithm must be performed:

1. Given the basic solution for the prescribed fault displacement, the parameters in Eq. (20) – (22) are determined.
2. The corrected distribution of the bending strains is calculated according to the relation

$$\varepsilon_b(x) = \frac{M(x)}{EI(x)}\frac{D}{2} \tag{30}$$

3. The corrected maximal bending and total strains are then evaluated:

$$\varepsilon_b = \frac{M(x_{\max})}{EI(x_{\max})}\frac{D}{2},\ \varepsilon_{\max} = \varepsilon_b + \varepsilon_{a,\max} \tag{31}$$

The strain correction procedure was applied to the pipeline-fault intersection analysis of section 3.2. Figure 10 illustrates the corrected stiffness distribution for the case $\beta = 90^0$, $\Delta / D = 2$. The lengths of the curved segments AB and BC were $L_1 = L_2 = L = 9.91$ m. The parameters of Eq. (20) – (22) were found to be $C_3 = 2.18$, $l_p = 6.05$ m.

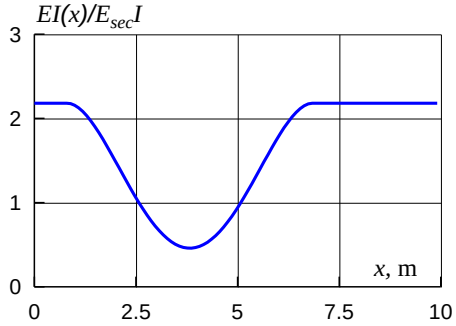

Figure 10: The corrected stiffness distribution on segments AB and BC for $\beta = 90^0$, $\Delta / D = 2$.

Figure 11 illustrates the application of the correction procedure to the analytical solution for crossing angles $\beta = 30^0$, 45^0, 60^0, 80^0 and 90^0. The maximal strains obtained with analytical model without correction (curves 1), analytical model with strain correction (curves 2), and finite element model (curves 3) are plotted against the fault displacement. It can be noted that the suggested correction procedure substantially improves the maximal strain assessment for crossing angles close to 90^0 with slight overestimate for small and moderate crossing angles.

In figure 12 the comparison of the bending strain distributions in the near fault zone is presented for $\Delta / D = 0.5, 1$ and 2 m. The numbering of curves corresponds to the figure 11. It can be concluded that the corrected strain distribution follows the exact (finite element) strain distribution quite closely for all three values of the fault displacement. In particular, for moderate strains the plastic strains are small and strain concentration is not observed. As the plastic strains caused by bending become large, the unevenness of strain distribution also grows and the effect of strain concentration is accounted for.

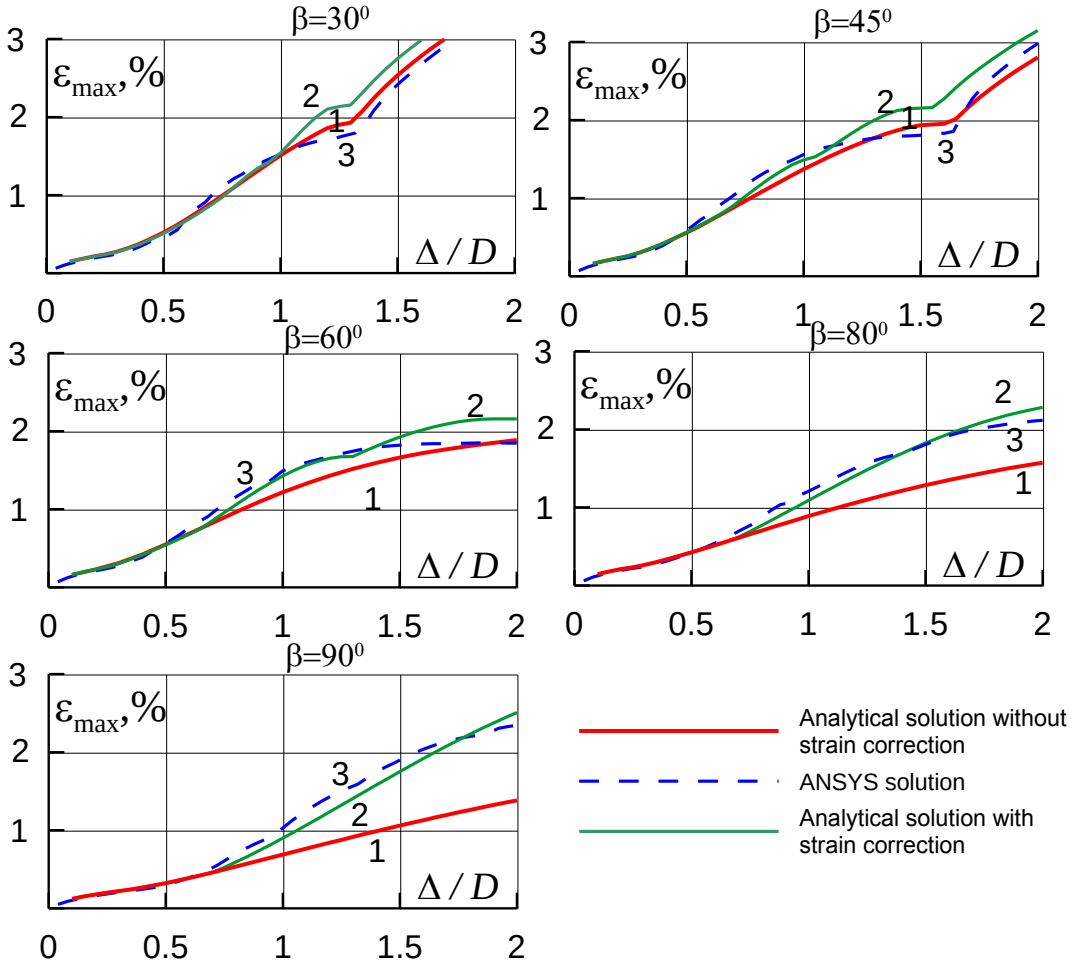

Figure 11: Evolution of the maximal strains with the fault displacement for different fault intersection angles.

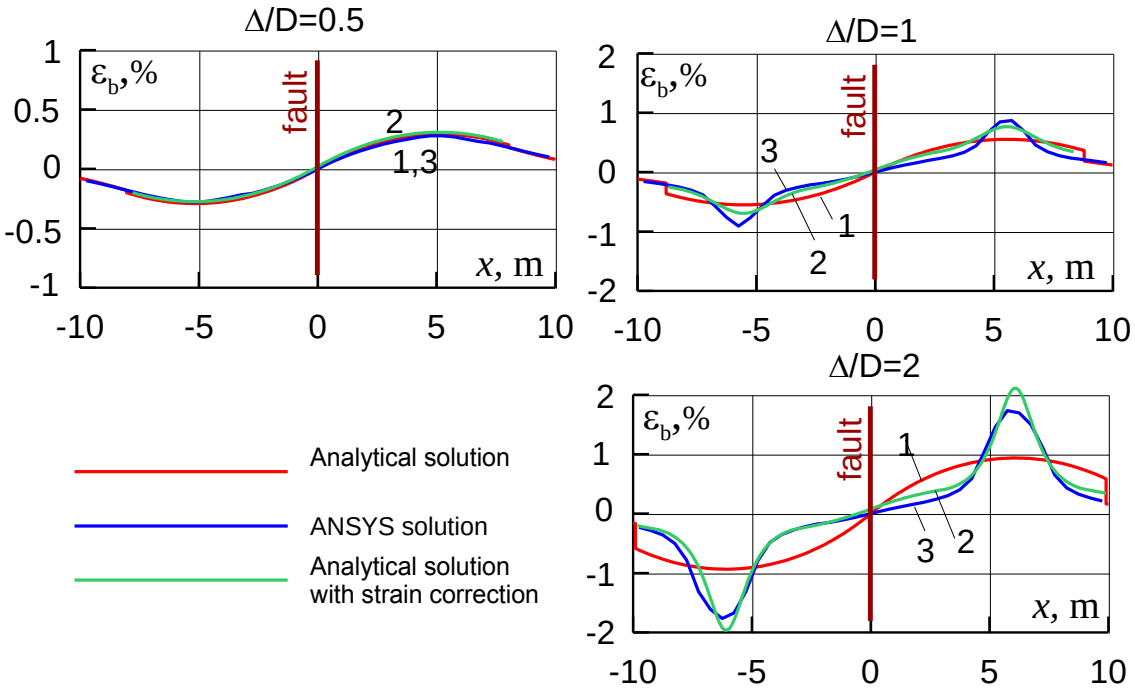

Figure 12: Bending strain distributions in the near fault zone for the case $\beta = 90^0$.

5 CONCLUSIONS

The analytical model for stress-strain analysis of pipelines crossing active faults described in paper [6] is outlined. The comparison of the numerical results obtained with the analytical model to the results of a more rigorous finite element model is performed for the case of strike-slip fault crossing at various intersection angles. The detailed analysis of the strain distributions in the near fault zone revealed the limitations of the analytical model. In particular, for the fault crossing angle close to 90^0 the difference in maximal strains is substantial for large fault displacements.

Based on the performed analysis, a strain correction procedure is suggested. The results of the numerical simulation with the use of strain correction show good correspondence with the finite element results in the range of fault intersection angles from 30^0 to 90^0 and fault displacements from 0 to 2*D* (where *D* is the pipe diameter). Thus, it can be concluded that the suggested procedure of strain correction extends the applicability of the original analytical model to the practically important case of pipeline crossing active fault at an angle close to 90^0. The main advantage of the proposed procedure is its simplicity and direct applicability to the original pipeline model. The main drawbacks, as they are seen to the authors, are the mostly empirical character of the correction procedure and the need to use an exact numerical solution for preliminary calibration of the strain correction parameters.

REFERENCES

[1] M.J. O'Rourke, X. Liu, *Response of Buried Pipelines Subject to Earthquake Effects*, MCEER, New York, 1999.

[2] N.M. Newmark, W.J. Hall, Pipeline design to resist large fault displacement. In: *Proceedings of the US National Conference on Earthquake Engineering.* Ann Arbor: University of Michigan, 416–425, 1975.

[3] R.P. Kennedy, A.W. Chow, R.A. Williamson, Fault movement effects on buried oil pipeline. *Transport Eng. J. ASCE,* **103**, 617-633, 1977.

[4] L.R.L. Wang, Y.A. Yeh, A refined seismic analysis and design of buried pipeline for fault movement. *Earthquake Eng. Struct. Dyn.* **13**, 75-96, 1985.

[5] D.K. Karamitros, G.D. Bouckovalas, G.P. Kouretzis, Stress analysis of buried steel pipelines at strike-slip fault crossings. *Soil Dynamics and Earthquake Engineering*, **27**, 200-211, 2007.

[6] O.V. Trifonov, V.P. Cherniy, A semi-analytical approach to a nonlinear stress-strain analysis of buried steel pipelines crossing active faults. *Soil Dynamics and Earthquake Engineering*, **30**, 1298-1308, 2010.

[7] Ansys Inc. *ANSYS Release 12.1 Documentation*, 2009.

[8] American Lifelines Alliance. *Guidelines for the design of buried steel pipes*. ASCE, 2001.